

**<Supporting Information>**

**Cation-size-controlled assembly of Ni(Ac)<sub>2</sub>–1,4-H<sub>2</sub>NDC system: geminal dicationic ionothermal syntheses, crystal structures and magnetic properties**

**Bing An,<sup>a</sup> Yan Bai\*,<sup>a,b</sup> Jun-Li Wang<sup>a</sup> and Dong-Bin Dang\*<sup>a</sup>**

<sup>a</sup> Henan Key Laboratory of Polyoxometalate Chemistry. Institute of Molecular and Crystal Engineering, College of Chemistry and Chemical Engineering, Henan University, Kaifeng 475004, P.R. China.

<sup>b</sup> State Key Laboratory of Coordination Chemistry, Nanjing University, Nanjing 210093, P.R. China.

**Contents:**

Section 1 Experimental Section.

Section 2 Supplementary Structural Tables.

Section 3 Supplementary Structural Figures.

Section 4 Additional Measurements.

Section 5 Magnetic properties.

## **1. Experimental Section.**

### **1.1 Materials and methods**

All reagents were commercially available and used without further purification. The ionic liquids,  $C_3(\text{MIm})_2\text{Br}_2$ ,  $C_4(\text{MIm})_2\text{Br}_2$ ,  $C_5(\text{MIm})_2\text{Br}_2$  and  $C_6(\text{MIm})_2\text{Br}_2$ , were synthesized according to the literature method.<sup>1, 2</sup> Elemental analyses (C, H and N) were carried out on a Perkin-Elmer 240C analytical instrument. IR spectra were recorded in KBr pellets with a Nicolet 170 SXFT-IR spectrophotometer in the 4000–400  $\text{cm}^{-1}$  region. X-ray powder diffraction patterns were recorded on a D/max- $\gamma$  A rotating anode X-ray diffractometer with Cu sealed tube ( $\lambda = 1.54178 \text{ \AA}$ ). Magnetic susceptibility data on crushed single crystals were collected over the temperature range 1.8–300.0 K using a Quantum Design MPMS-5S superconducting quantum interference device (SQUID) magnetometer. The thermogravimetric analyses were carried out under nitrogen condition on a Perkin-Elmer-7 thermal analyzer at a heating rate of 10°C/min from 25 to 800 °C.

## 1.2 Syntheses of 1-4

**[C<sub>3</sub>(MIm)<sub>2</sub>][Ni(1,4-ndc)Br]<sub>2</sub> 1.** A mixture of 1,4-H<sub>2</sub>NDC (1 mmol), Ni(Ac)<sub>2</sub>·6H<sub>2</sub>O (1.5 mmol) and C<sub>3</sub>(MIm)<sub>2</sub>Br<sub>2</sub> (1.5 g) was transferred to a 25 mL Teflon-lined steel autoclave and kept at 180 °C for 3 days under autogenous pressure. After naturally cooled down to room temperature, green crystals were obtained and washed with methanol. Yields (based on 1,4-H<sub>2</sub>NDC): ca. 75%. Anal. Calcd (%) for C<sub>35</sub>H<sub>30</sub>Br<sub>2</sub>N<sub>4</sub>Ni<sub>2</sub>O<sub>8</sub>: C, 46.10; H, 3.32; N, 6.14. Found: C, 46.25; H, 3.25; N, 6.09. IR (cm<sup>-1</sup>, KBr pellet): 3429(w), 3150(w), 3100(w), 3070(w), 2956(w), 1618(vs), 1588(vs), 1564(s), 1512(w), 1468(m), 1425(s), 1371(vs), 1269(w), 1215(w), 1163(m), 1112(w), 1032(w), 855(w), 826(m), 794(w), 764(m), 746(w), 670(w), 621(w), 574(m), 522(w), 455(w).

**[C<sub>4</sub>(MIm)<sub>2</sub>][Ni(1,4-ndc)Br]<sub>2</sub> 2.** The reaction procedure was carried out in a similar manner to that of **1**, except that C<sub>4</sub>(MIm)<sub>2</sub>Br<sub>2</sub> was used instead of C<sub>3</sub>(MIm)<sub>2</sub>Br<sub>2</sub>. The product, **2**, was obtained in 69% yield. Anal. Calcd(%) for C<sub>18</sub>H<sub>16</sub>BrN<sub>2</sub>NiO<sub>4</sub>: C, 46.70; H, 3.48; N, 6.05. Found: C, 46.57; H, 3.42; N, 6.18. IR (cm<sup>-1</sup>, KBr pellet): 3429(w), 3148(w), 3100(w), 3070(w), 2958(w), 1616(vs), 1588(vs), 1568(s), 1512(w), 1468(m), 1424(s), 1370(vs), 1271(w), 1213(w), 1163(m), 1112(w), 1032(w), 855(w), 826(m), 794(w), 764(m), 746(w), 670(w), 621(w), 574(m), 522(w), 455(w).

**[Ni<sub>3</sub>(1,4-ndc)<sub>4</sub>(MIm-C<sub>5</sub>Ml)<sub>2</sub>(H<sub>2</sub>O)<sub>2</sub>] 3.** The reaction procedure was carried out in a similar manner to that of **1**, except that C<sub>5</sub>(MIm)<sub>2</sub>Br<sub>2</sub> was used instead of C<sub>4</sub>(MIm)<sub>2</sub>Br<sub>2</sub>. The product, **3**, was obtained in 71% yield (based on 1,4-H<sub>2</sub>NDC). Anal. Calcd(%) for C<sub>72</sub>H<sub>66</sub>N<sub>8</sub>Ni<sub>3</sub>O<sub>18</sub>: C, 57.37; H, 4.41; N, 7.43. Found: C, 57.26; H, 4.50; N, 7.54. IR (cm<sup>-1</sup>, KBr pellet): 3430(w), 3156(w), 3107(w), 3024(w), 2920(w), 1626(vs), 1588(vs), 1563(s), 1509(w), 1459(m), 1410(s), 1365(vs), 1263(w), 1212(w), 1172(m), 1109(w), 1031(w), 865(w), 808(m), 790(m), 746(w), 662(w), 631(w), 557(m), 522(w), 451(w).

**[Ni<sub>3</sub>(1,4-ndc)<sub>4</sub>(MIm-C<sub>6</sub>Ml)<sub>2</sub>(H<sub>2</sub>O)<sub>2</sub>] 4.** The reaction procedure was carried out in a similar manner to that of **1**, except that C<sub>6</sub>(MIm)<sub>2</sub>Br<sub>2</sub> was used instead of C<sub>5</sub>(MIm)<sub>2</sub>Br<sub>2</sub>. The product, **3**, was obtained in 74% yield (based on 1,4-H<sub>2</sub>NDC). Anal. Calcd(%) for C<sub>74</sub>H<sub>70</sub>N<sub>8</sub>Ni<sub>3</sub>O<sub>18</sub>: C, 57.88; H, 4.60; N, 7.30. Found: C, 57.73; H, 4.46; N, 7.45. IR (cm<sup>-1</sup>, KBr pellet): 3427(w), 3162(w), 3109(w), 3037(w), 2939(w), 1619(vs), 1571(vs), 1511(w), 1459(m), 1410(s), 1365(vs), 1263(w), 1210(w), 1153(m), 1108(w), 1030(w), 945(w), 863(w), 805(m), 791(m), 748(w), 665(w), 626(w), 560(m), 520(w), 451(w).

### X-ray crystal structure determination

X-ray single crystal diffraction data for polymers **1–4** were collected on a Bruker Apex-II CCD detector using graphite monochromatized Mo-K $\alpha$  radiation ( $\lambda = 0.71073 \text{ \AA}$ ) using SMART and SAINT programs. Routine Lorentz and polarization corrections were applied. The structures were solved by direct methods of SHELXS-97 and refined by full-matrix least-squares method using the SHELXL-97 program package.<sup>3</sup> All of the non-hydrogen atoms were refined with anisotropic thermal displacement coefficients. Hydrogen atoms were assigned to calculated positions using a riding model with appropriately fixed isotropic thermal parameters.

Polymers **1** and **2** both crystallize in the space group of  $P2_1/n$ . The  $[\text{C}_3(\text{MIm})_2]^{2+}$  was refined as disordered with the site occupancy factor (s.o.f.) of 0.5 for all atoms. N1, C13 and C15 from  $[\text{C}_4(\text{MIm})_2]^{2+}$  are rotationally disordered over two orientations in the refined ratio 0.5 : 0.5. Polymers **3** and **4** crystallize in the space group of  $P2_1/n$  and  $P2_1/c$ , respectively. The detailed crystallographic data and structure refinement parameters are summarized in Table S1. Selected bond distances, bond angles and hydrogen bonding interactions for **1–4** are listed in Tables S2–S13.

### References:

1. Z. Zeng, B. S. Phillips, J.-C. Xiao and J. n. M. Shreeve, *Chem. Mater.*, 2008, **20**, 2719-2726.
2. H. Tadesse, A. J. Blake, N. R. Champness, J. E. Warren, P. J. Rizkallah and P. Licence, *CrystEngComm.*, 2012, **14**, 4886-4893.
3. (a) G. M. Sheldrick, SHELXS-97, Programs for X-ray Crystal Structure Solution; University of Göttingen: Göttingen, Germany, 1997. (b) G. M. Sheldrick, SHELXL-97, Programs for X-ray Crystal Structure Refinement; University of Göttingen: Göttingen, Germany, 1997

## 2. Supplementary Structural Tables.

**Table S1** Crystal data for polymers **1–4**

	<b>1</b>	<b>2</b>	<b>3</b>	<b>4</b>
Chemical formula	C <sub>35</sub> H <sub>30</sub> Br <sub>2</sub> N <sub>4</sub> Ni <sub>2</sub> O <sub>8</sub>	C <sub>18</sub> H <sub>16</sub> BrN <sub>2</sub> NiO <sub>4</sub>	C <sub>72</sub> H <sub>66</sub> N <sub>8</sub> Ni <sub>3</sub> O <sub>18</sub>	C <sub>74</sub> H <sub>70</sub> N <sub>8</sub> Ni <sub>3</sub> O <sub>18</sub>
Formula Mass	911.87	462.95	1507.46	1535.51
Temperature/K	296(2)	296(2)	296(2)	296(2)
Crystal system	Monoclinic	Monoclinic	Monoclinic	Monoclinic
Space group	P2 <sub>1</sub> /n	P2 <sub>1</sub> /n	P2 <sub>1</sub> /n	P2 <sub>1</sub> /c
<i>a</i> /Å	10.0658(7)	10.0037(5)	12.547(7)	15.2845(12)
<i>b</i> /Å	15.3720(10)	15.4731(8)	12.979(7)	14.8122(12)
<i>c</i> /Å	11.0263(8)	11.1313(6)	24.368(13)	16.9361(17)
$\beta^{\circ}$	92.7650(10)	92.1400(10)	117.7970(10)	117.9430(10)
<i>V</i> /Å <sup>3</sup>	1704.1(2)	1721.79(15)	3276.3(4)	3387.3(5)
<i>Z</i>	2	4	2	2
<i>D</i> / <sup>o</sup> g·cm <sup>-3</sup>	1.777	1.786	1.528	1.506
	-10 ≤ <i>h</i> ≤ 11	-8 ≤ <i>h</i> ≤ 11	-17 ≤ <i>h</i> ≤ 18	-17 ≤ <i>h</i> ≤ 18
Limiting indices	-18 ≤ <i>k</i> ≤ 17	-18 ≤ <i>k</i> ≤ 18	-10 ≤ <i>k</i> ≤ 18	-17 ≤ <i>k</i> ≤ 17
	-12 ≤ <i>l</i> ≤ 13	-12 ≤ <i>l</i> ≤ 13	-18 ≤ <i>l</i> ≤ 18	-12 ≤ <i>l</i> ≤ 20
Measured reflections	2994	3027	5774	5969
Data/restraints/parameters	2152/24/223	2420/26/244	4169/18/458	3802/38/484
$\mu/\text{mm}^{-1}$	3.509	3.475	0.935	0.906
GOF on <i>F</i> <sup>2</sup>	1.072	1.064	1.052	1.036
<i>R</i> <sub>int</sub>	0.0491	0.0331	0.0584	0.0739
<i>R</i> <sub>1</sub> , <i>wR</i> <sub>2</sub> [ <i>I</i> > 2σ( <i>I</i> )]	0.0500, 0.1278	0.0382, 0.0956	0.0456, 0.0966	0.0489, 0.0872
<i>R</i> <sub>1</sub> , <i>wR</i> <sub>2</sub> [all data]	0.0774, 0.1389	0.0521, 0.1004	0.0742, 0.1058	0.0955, 0.0976
Largest residuals/e Å <sup>-3</sup>	0.812/-0.700	1.255/-0.625	0.626/-0.498	0.440/-0.405

**Table S2.** Selected bond lengths ( $\text{\AA}$ ) for polymer **1**.

bond	length	bond	length
Ni1(1)–O(2A)	2.019(4)	Ni1(1)–O(1)	2.014(4)
Ni1(1)–O(3B)	2.018(4)	Ni1(1)–O(4C)	2.024(4)
Ni1(1)–Br(1)	2.4282(9)		

Symmetry codes: A,  $1 - x, 1 - y, 1 - z$ ; B,  $1/2 + x, 1/2 - y, -1/2 + z$ ; C,  $1/2 - x, 1/2 + y, 3/2 - z$ .

**Table S3.** Selected bond angles ( $^{\circ}$ ) for polymer **1**.

bond angle	degree	bond angle	degree
O(1)–Ni(1)–O(3B)	88.74(18)	O(1)–Ni(1)–O(2A)	161.91(17)
O(3B)–Ni(1)–O(2A)	88.43(18)	O(1)–Ni(1)–O(4C)	88.22(18)
O(3B)–Ni(1)–O(4C)	161.92(17)	O(2A)–Ni(1)–O(4C)	88.95(18)
O(1)–Ni(1)–Br(1)	101.17(13)	O(3B)–Ni(1)–Br(1)	99.21(13)
O(2A)–Ni(1)–Br(1)	96.92(12)	O(4C)–Ni(1)–Br(1)	98.86(12)

Symmetry codes: A,  $1 - x, 1 - y, 1 - z$ ; B,  $1/2 + x, 1/2 - y, -1/2 + z$ ; C,  $1/2 - x, 1/2 + y, 3/2 - z$ .

**Table S4.** Hydrogen bond parameters ( $\text{\AA}$ ,  $^\circ$ ) of polymer **1**.

D–H…A	D(D–H)	d(H…A)	d(D…A)	$\angle(\text{DHA})$	Symmetry transformation for A
C(13)–H(13A)…Br(1)	0.96	2.82	3.709(19)	154	$1/2 - x, -1/2 + y, 1/2 - z$
C(13)–H(13C)…O(1)	0.96	2.43	3.19(2)	136	$1/2 + x, 1/2 - y, -1/2 + z$
C(15)–H(15A)…Br(1)	0.96	2.83	3.791(13)	175	$1 - x, 1 - y, 1 - z$
C(19)–H(19A)…Br(1)	0.96	2.92	3.52(3)	122	
C(19)–H(19A)…O(3)	0.96	2.56	3.47(3)	158	$1/2 + x, 1/2 - y, -1/2 + z$
C(20)–H(20A)…Br(1)	0.96	2.92	3.849(15)	164	$1 - x, 1 - y, 1 - z$

**Table S5.** Selected bond lengths ( $\text{\AA}$ ) for polymer **2**.

bond	length	bond	length
Ni1(1)–O(2A)	2.017(3)	Ni1(1)–O(1)	2.018(3)
Ni1(1)–O(3B)	2.027(3)	Ni1(1)–O(4C)	2.027(3)
Ni1(1)–Br(1)	2.4320(7)		

Symmetry codes: A,  $1 - x, -y, 1 - z$ ; B,  $-1/2 + x, 1/2 - y, 1/2 + z$ ; C,  $3/2 - x, -1/2 + y, 1/2 - z$ .

**Table S6.** Selected bond angles ( $^{\circ}$ ) for polymer **2**.

bond angle	degree	bond angle	degree
O(1)–Ni(1)–O(2A)	162.38(10)	O(1)–Ni(1)–O(3B)	88.37(11)
O(2A)–Ni(1)–O(3B)	88.31(11)	O(1)–Ni(1)–O(4C)	88.84(11)
O(2A)–Ni(1)–O(4C)	89.08(11)	O(3B)–Ni(1)–O(4D)	162.29(11)
O(1)–Ni(1)–Br(1)	97.66(7)	O(2A)–Ni(1)–Br(1)	99.96(7)
O(3B)–Ni(1)–Br(1)	99.08(8)	O(4C)–Ni(1)–Br(1)	98.63(8)

Symmetry codes: A,  $1 - x, -y, 1 - z$ ; B,  $-1/2 + x, 1/2 - y, 1/2 + z$ ; C,  $3/2 - x, -1/2 + y, 1/2 - z$ .

**Table S7.** Hydrogen bond parameters ( $\text{\AA}$ ,  $^\circ$ ) of polymer **2**.

D–H…A	D(D–H)	d(H…A)	d(D…A)	$\angle$ (DHA)	Symmetry transformation for A
C(13)–H(13B)…O(4)	0.96	2.43	3.226(12)	141	$-1 + x, y, z$
C(13)–H(13B)…O(2)	0.96	2.43	3.245(13)	142	$-1/2 + x, 1/2 - y, -1/2 + z$
C(13')–H(13D)…Br(1)	0.96	2.69	3.585(13)	155	$1/2 + x, 1/2 - y, -1/2 + z$
C(13')–H(13F)…O(2)	0.96	2.40	3.173(12)	138	$-1/2 + x, 1/2 - y, -1/2 + z$
C(14)–H(14A)…Br(1)	0.93	2.73	3.637(10)	165	

**Table S8.** Selected bond lengths ( $\text{\AA}$ ) for polymer **3**.

bond	length	bond	length
Ni(1)–O(1)	2.007(3)	Ni(1)–O(7C)	2.016(2)
Ni(1)–O(6B)	2.038(2)	Ni(1)–O(4A)	2.046(3)
Ni(1)–N(1)	2.055(3)	Ni(1)–O(1W)	2.129(2)
Ni(2)–O(5)	2.043(2)	Ni(2)–O(8D)	2.071(2)
Ni(2)–O(1W)	2.085(2)		

Symmetry codes: A,  $3/2 - x, -1/2 + y, 3/2 - z$ ; B,  $2 - x, 1 - y, 1 - z$ ; C,  $-1/2 + x, 1/2 - y, -1/2 + z$ ; D,  $5/2 - x, 1/2 + y, 3/2 - z$ .

**Table S9.** Selected bond angles ( $^{\circ}$ ) for polymer **3**.

bond angle	degree	bond angle	degree
O(1)–Ni(1)–O(7C)	176.26(13)	O(1)–Ni(1)–O(6B)	86.98(12)
O(7C)–Ni(1)–O(6B)	90.25(12)	O(1)–Ni(1)–O(4A)	93.94(13)
O(7C)–Ni(1)–O(4A)	88.64(12)	O(6B)–Ni(1)–O(4A)	175.69(11)
O(1)–Ni(1)–N(1)	88.46(12)	O(7C)–Ni(1)–N(1)	88.94(12)
O(6B)–Ni(1)–N(1)	88.16(11)	O(4A)–Ni(1)–N(1)	87.66(11)
O(1)–Ni(1)–O(1W)	90.08(10)	O(7C)–Ni(1)–O(1W)	92.69(10)
O(6B)–Ni(1)–O(1W)	95.76(9)	O(4A)–Ni(1)–O(1W)	88.46(10)
N(1)–Ni(1)–O(1W)	175.75(10)	O(5)–Ni(2)–O(5B)	180.000(1)
O(5)–Ni(2)–O(8D)	94.00(10)	O(5)–Ni(2)–O(1W)	86.87(8)
O(5)–Ni(2)–O(8C)	86.00(10)	O(8D)–Ni(2)–O(1W)	87.68(9)
O(8D)–Ni(2)–O(8C)	180.000(1)	O(5)–Ni(2)–O(1WB)	93.13(8)
O(5B)–Ni(2)–O(1W)	93.13(8)	O(8D)–Ni(2)–O(1WB)	92.32(9)
O(8C)–Ni(2)–O(1W)	92.32(9)	O(1W)–Ni(2)–O(1WB)	180.000(1)

Symmetry codes: A,  $3/2 - x, -1/2 + y, 3/2 - z$ ; B,  $2 - x, 1 - y, 1 - z$ ; C,  $-1/2 + x, 1/2 - y, -1/2 + z$ ; D,  $5/2 - x, 1/2 + y, 3/2 - z$ .

**Table S10.** Hydrogen bond parameters ( $\text{\AA}$ ,  $^\circ$ ) of polymer **3**.

D–H…A	D(D–H)	d(H…A)	d(D…A)	$\angle$ (DHA)	Symmetry transformation for A
O(1W)–H(1WA)…O(2)	0.97	1.93	2.726(4)	138	
O(1W)–H(1WB)…O(3)	0.97	1.70	2.576(4)	149	$3/2 - x, -1/2 + y, 3/2 - z$
C(4)–H(4A)…O(1)	0.93	2.28	2.627(5)	102	
C(11)–H(11A)…O(2)	0.93	2.28	2.922(5)	126	
C(20)–H(20A)…O(8)	0.93	2.39	2.939(5)	118	
C(23)–H(23A)…O(6)	0.93	2.53	2.994(4)	111	
C(30)–H(30B)…N(2)	0.97	2.57	2.977(7)	105	
C(32)–H(32B)…O(3)	0.97	2.47	3.432(7)	174	$1 - x, 1 - y, 1 - z$
C(35)–H(35A)…O(5)	0.93	2.28	3.163(5)	159	$-1/2 + x, 1/2 - y, -1/2 - z$

**Table S11.** Selected bond lengths ( $\text{\AA}$ ) for polymer **4**.

bond	length	bond	length
Ni(1)–O(7B)	2.016(3)	Ni(1)–O(3A)	2.018(3)
Ni(1)–O(1)	2.041(3)	Ni(1)–O(6)	2.042(3)
Ni(1)–N(1)	2.064(3)	Ni(1)–O(1W)	2.114(2)
Ni(2)–O(5)	2.041(2)	Ni(2)–O(8B)	2.067(2)
Ni(2)–O(1W)	2.068(2)		

Symmetry codes: A,  $-1 - x, 1/2 + y, -1/2 - z$ ; B,  $-x, -1/2 + y, 1/2 - z$ ; C,  $-x, -y, -z$ ; D,  $x, 1/2 - y, -1/2 + z$ .

**Table S12.** Selected bond angles ( $^{\circ}$ ) for polymer 4.

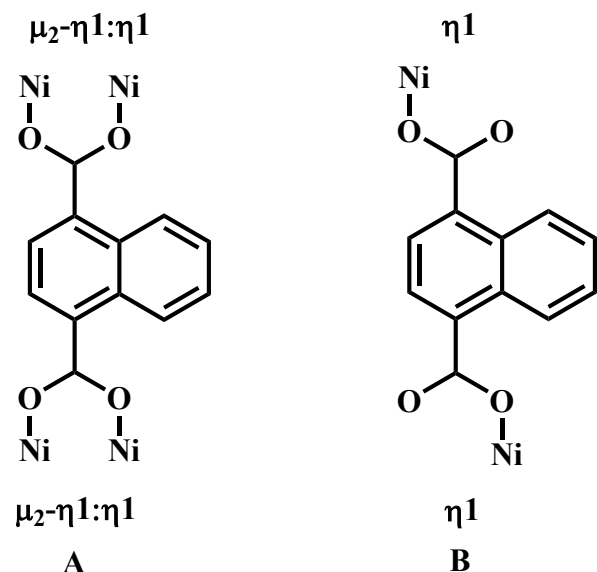
bond angle	degree	bond angle	degree
O(7B)–Ni(1)–O(3A)	174.05(12)	O(7B)–Ni(1)–O(1)	90.20(13)
O(3A)–Ni(1)–O(1)	89.26(13)	O(7B)–Ni(1)–O(6)	90.87(13)
O(3A)–Ni(1)–O(6)	89.53(13)	O(1)–Ni(1)–O(6)	178.29(12)
O(7B)–Ni(1)–N(1)	87.44(12)	O(3A)–Ni(1)–N(1)	86.62(12)
O(1)–Ni(1)–N(1)	87.53(11)	O(6)–Ni(1)–N(1)	91.19(11)
O(7B)–Ni(1)–O(1W)	94.02(10)	O(3A)–Ni(1)–O(1W)	91.90(11)
O(1)–Ni(1)–O(1W)	89.42(10)	O(6)–Ni(1)–O(1W)	91.84(10)
N(1)–Ni(1)–O(1W)	176.62(10)	O(5)–Ni(2)–O(5C)	180.0
O(5)–Ni(2)–O(8D)	87.16(10)	O(5)–Ni(2)–O(1WC)	89.45(9)
O(5)–Ni(2)–O(8B)	92.84(10)	O(5)–Ni(2)–O(1W)	90.55(9)
O(8D)–Ni(2)–O(8B)	180.00(17)	O(8D)–Ni(2)–O(1W)	85.46(9)
O(8B)–Ni(2)–O(1W)	94.54(9)	O(1WC)–Ni(2)–O(1W)	180.0

Symmetry codes: A,  $-1 - x, 1/2 + y, -1/2 - z$ ; B,  $-x, -1/2 + y, 1/2 - z$ ; C,  $-x, -y, -z$ ; D,  $x, 1/2 - y, -1/2 + z$ .

**Table S13.** Hydrogen bond parameters ( $\text{\AA}$ ,  $^\circ$ ) of polymer 4.

D–H…A	D(D–H)	d(H…A)	d(D…A)	$\angle$ (DHA)	Symmetry transformation for A
O(1W)–H(1WB)…O(2)	0.97	1.70	2.577(4)	148	
O(1W)–H(1WA)…O(4)	0.97	1.77	2.646(4)	148	$-1 - x, 1/2 + y, -1/2 - z$
C(8)–H(8A)…O(4)	0.93	2.46	3.045(6)	121	
C(11)–H(11A)…O(1)	0.93	2.46	2.995(6)	116	
C(20)–H(20A)…O(8)	0.93	2.38	2.941(5)	119	
C(23)–H(23A)…O(6)	0.93	2.54	2.997(5)	111	
C(25)–H(25A)…O(7)	0.93	2.47	2.930(6)	110	$-x, -1/2 + y, 1/2 - z$
C(26)–H(26A)…O(3)	0.93	2.59	2.973(6)	105	$-1 - x, 1/2 + y, -1/2 - z$
C(28)–H(28B)…O(3)	0.97	2.59	3.511(7)	158	$x, -1/2 - y, 1/2 + z$
C(33)–H(33B)…O(5)	0.97	2.47	3.412(7)	165	$-x, -1/2 + y, 1/2 - z$
C(37)–H(37A)…O(4)	0.96	2.20	3.122(6)	161	$1 + x, y, 1 + z$

### 3. Supplementary Structural Figures.



**Scheme S1.** The observed coordination modes of the  $1,4\text{-ndc}^{2-}$  ligands in **1-4**.

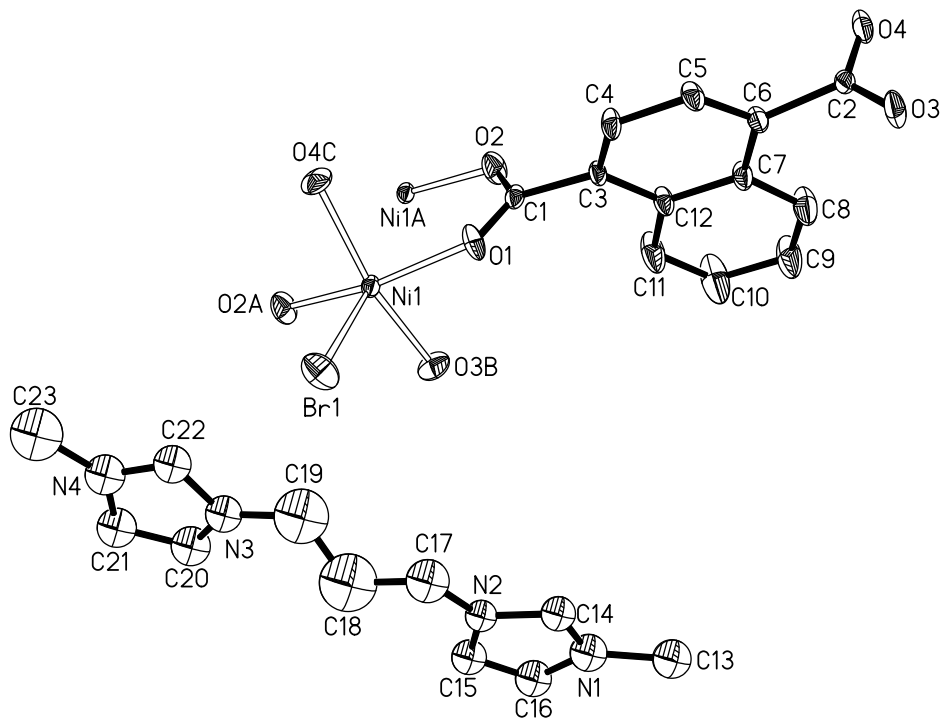


**Figure S1.** ORTEP view of **1** with the atom numbering scheme. The atoms are represented by 30% probability thermal ellipsoids. All the H atoms are omitted for clarity. Symmetry codes: A,  $1 - x, 1 - y, 1 - z$ ; B,  $1/2 + x, 1/2 - y, -1/2 + z$ ; C,  $1/2 - x, 1/2 + y, 3/2 - z$ .

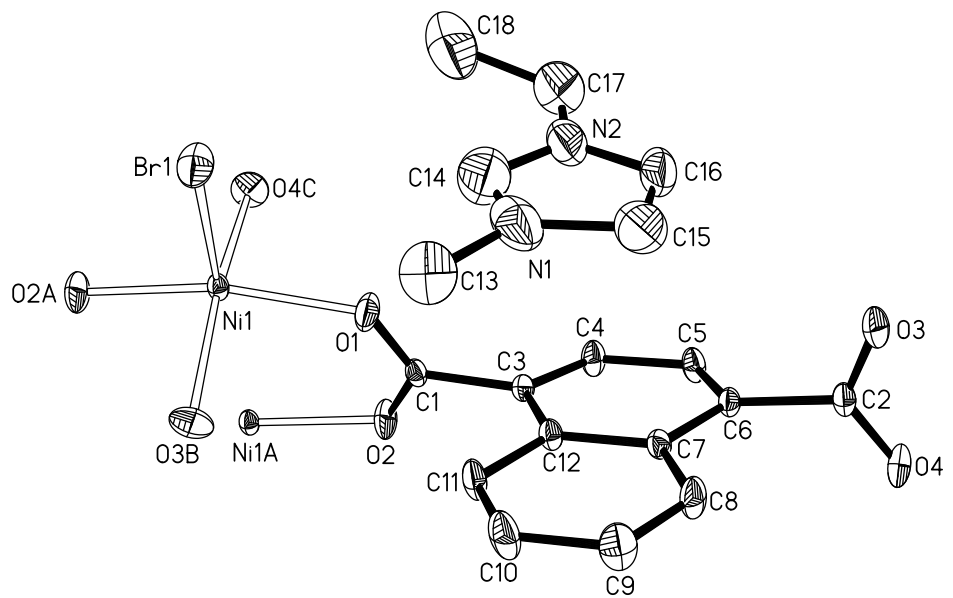


**Figure S2.** ORTEP view of **2** with the atom numbering scheme. The atoms are represented by 30% probability thermal ellipsoids. All the H atoms are omitted for clarity. Symmetry codes: A,  $1 - x, -y, 1 - z$ ; B,  $-1/2 + x, 1/2 - y, 1/2 + z$ ; C,  $3/2 - x, -1/2 + y, 1/2 - z$ .

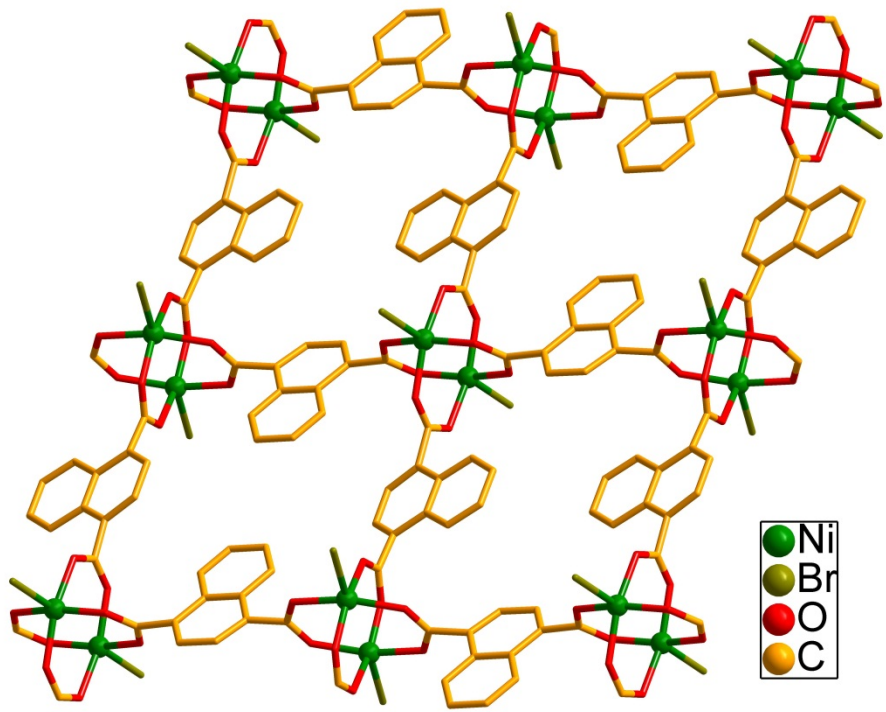


**Fig. S3** View of the 2D anionic layer of type A.

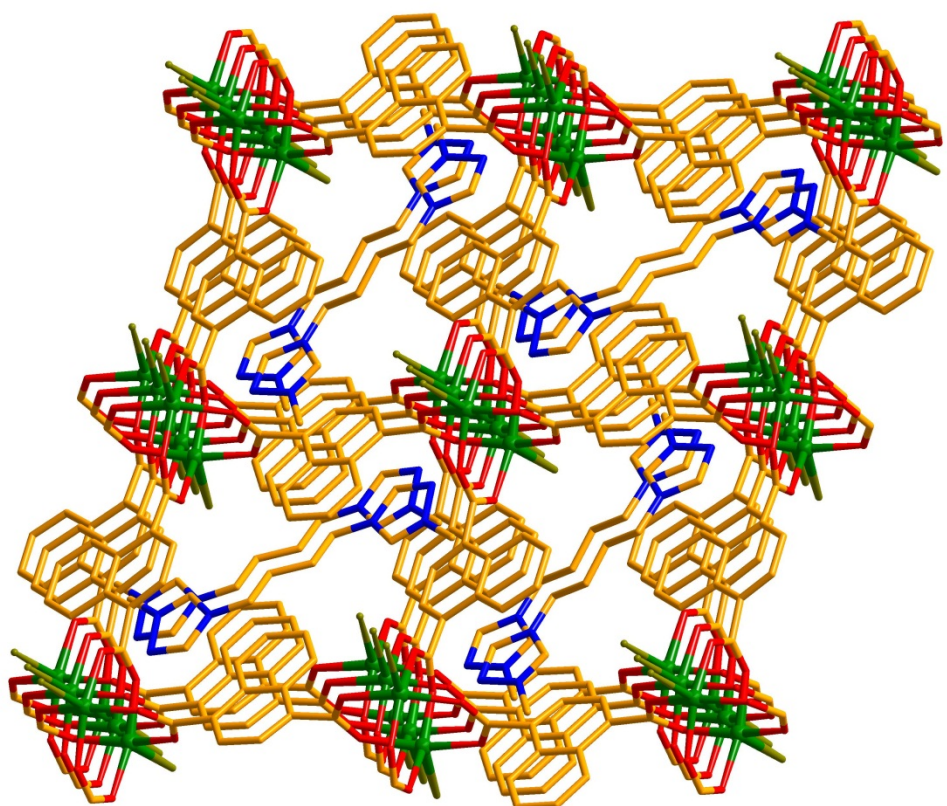


**Figure S4.** View of the 3D packing framework of **2** showing channels occupied by  $[C_4(MIm)_2]^{2+}$  cations.

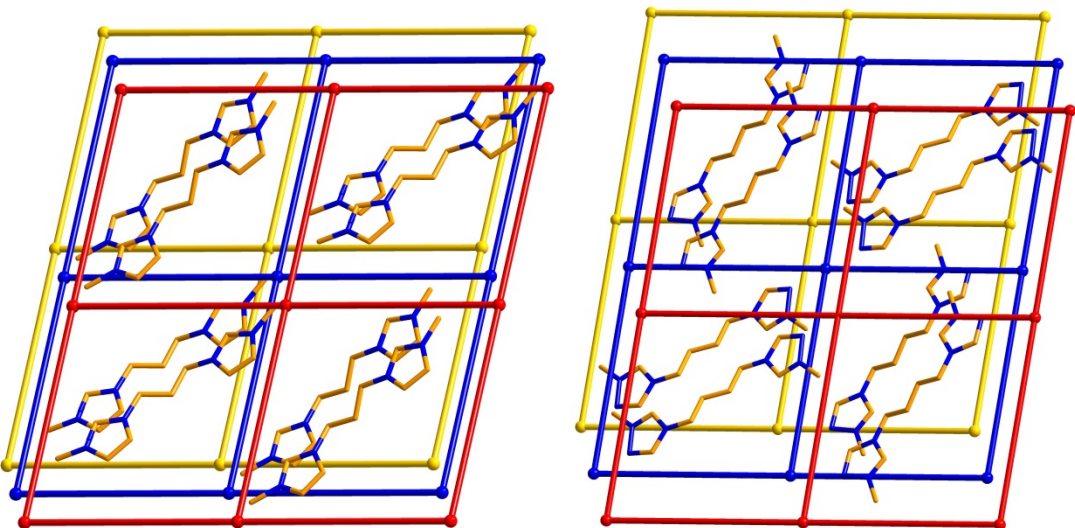


**Figure S5.** View of the topological structures of **1** (left) and **2** (right) showing channels occupied by  $[C_3(MIm)_2]^{2+}$  and  $[C_4(MIm)_2]^{2+}$  cations, respectively.

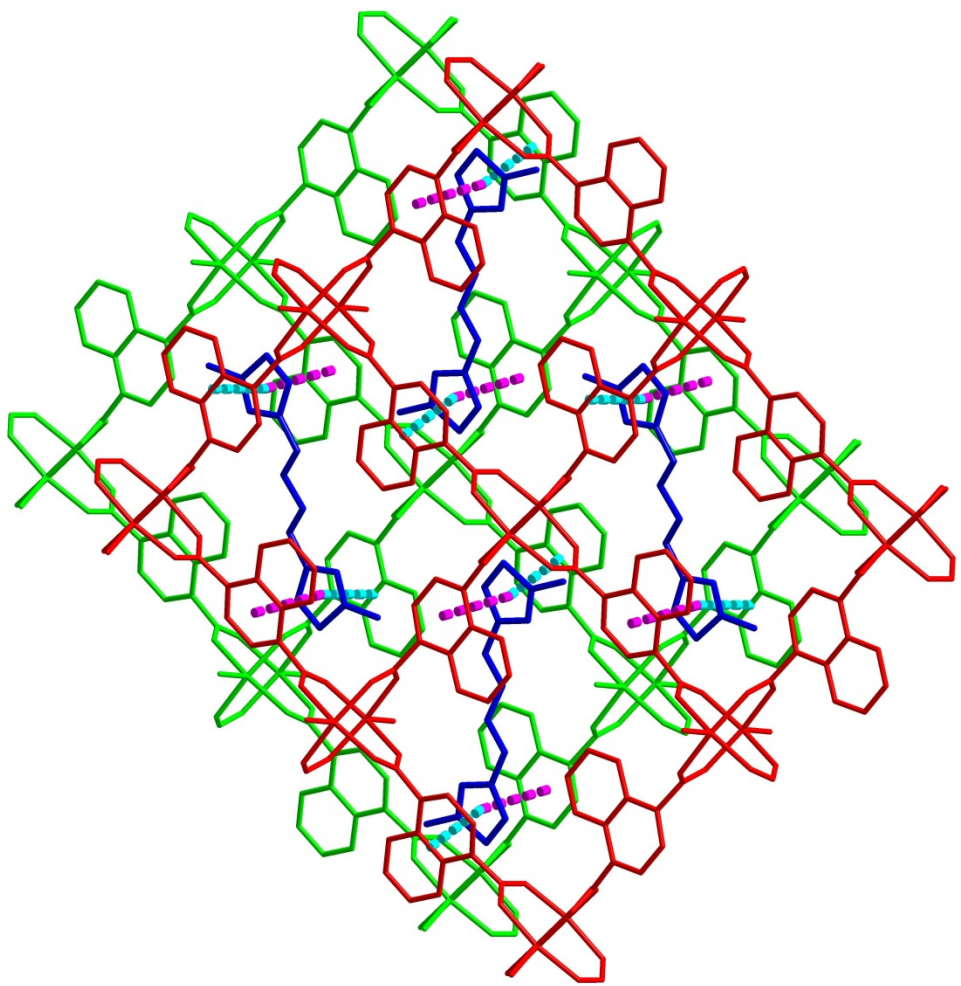


**Figure S6.** View of the 3D packing framework of **2** showing  $\pi\cdots\pi$  interactions between naphthalene rings of 1,4-ndc<sup>2-</sup> ligands and imidazole rings of [C<sub>4</sub>(MIm)<sub>2</sub>]<sup>2+</sup> cations.

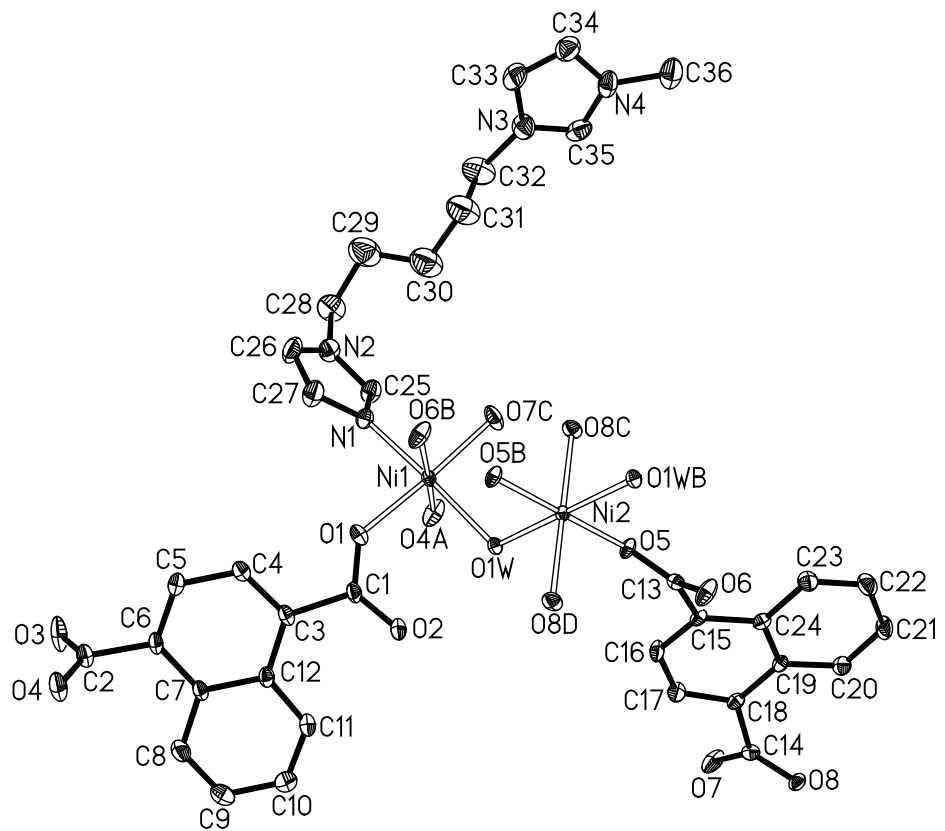


**Figure S7.** ORTEP view of **3** with the atom numbering scheme. The atoms are represented by 30% probability thermal ellipsoids. All the H atoms are omitted for clarity. Symmetry codes: A,  $3/2 - x, -1/2 + y, 3/2 - z$ ; B,  $2 - x, 1 - y, 1 - z$ ; C,  $-1/2 + x, 1/2 - y, -1/2 + z$ ; D,  $5/2 - x, 1/2 + y, 3/2 - z$ .

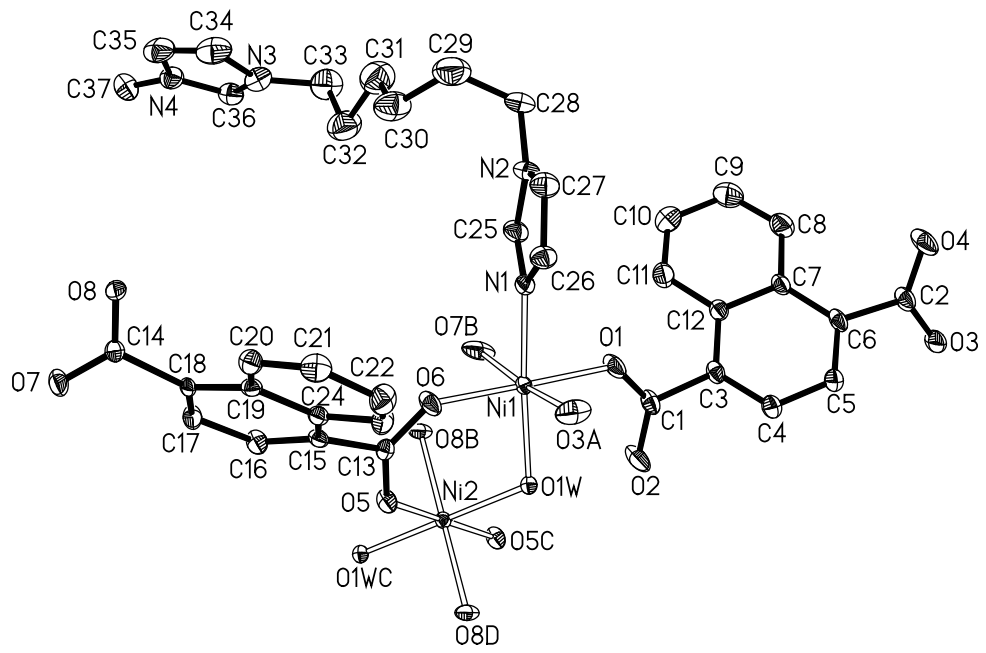


**Figure S8.** ORTEP view of **4** with the atom numbering scheme. The atoms are represented by 30% probability thermal ellipsoids. All the H atoms are omitted for clarity. Symmetry codes: A,  $-1 - x, 1/2 + y, -1/2 - z$ ; B,  $-x, -1/2 + y, 1/2 - z$ ; C,  $-x, -y, -z$ ; D,  $x, 1/2 - y, -1/2 + z$ .

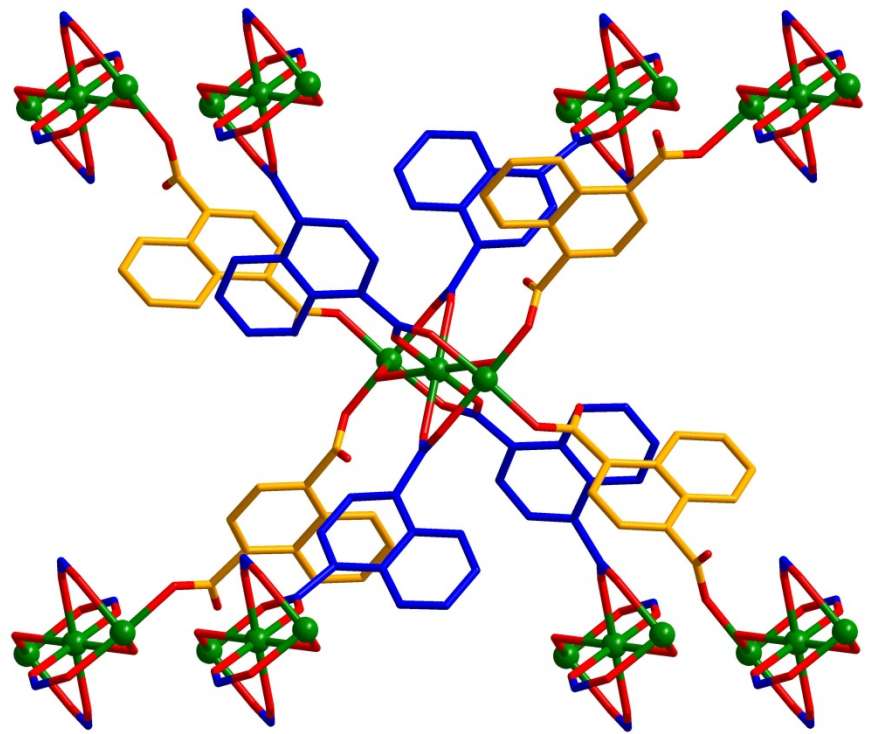


**Figure S9.** The trinuclear SBU with eight adjacent SBUs by eight linkages including four  $\mu_2\text{-}(\eta_1)\text{-}(\eta_1)$  bridging 1,4-ndc<sup>2-</sup> ligands and four  $\mu_4\text{-}(\mu_2\text{-}\eta_1\text{:}\eta_1)\text{-}(\mu_2\text{-}\eta_1\text{:}\eta_1)$  bridging 1,4-ndc<sup>2-</sup> ligands.

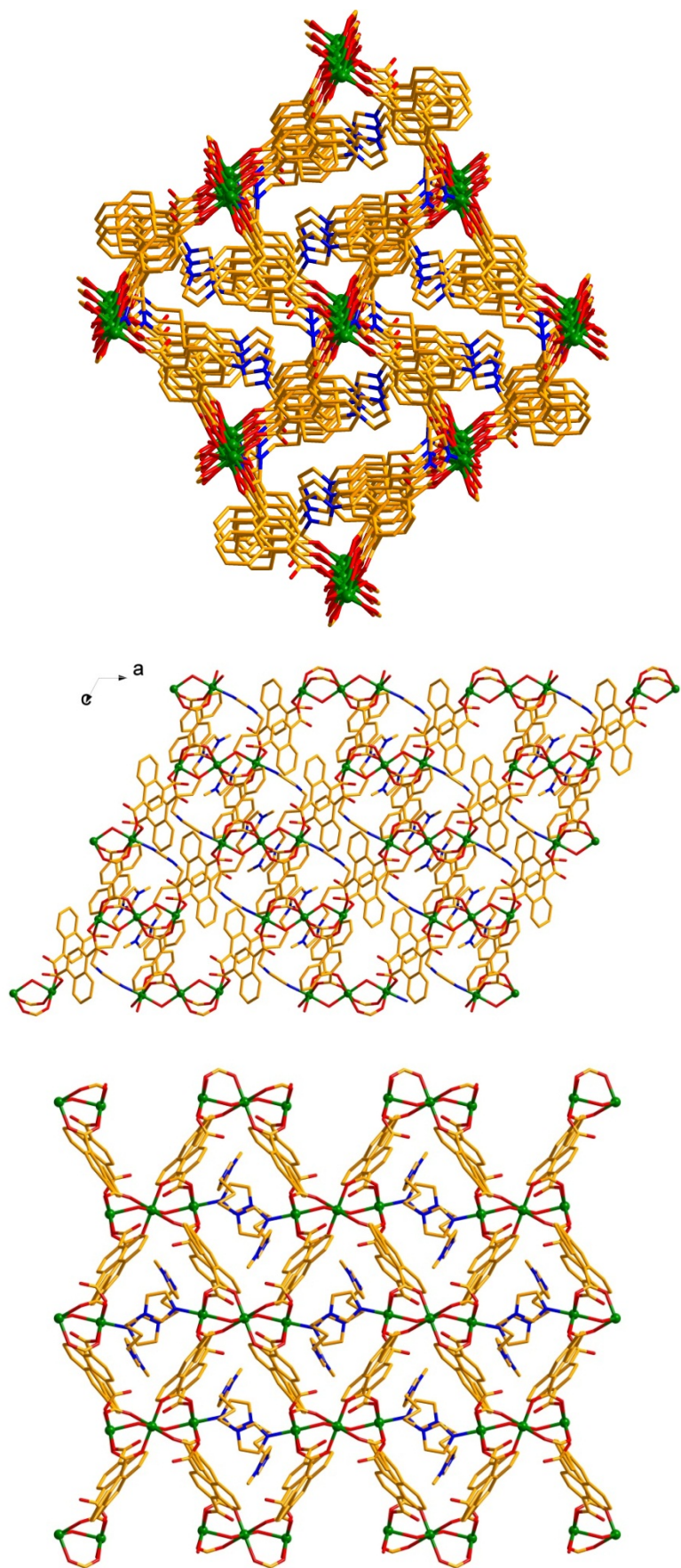


**Figure S10.** Illustration of 3D network seen from different orientations in 3.

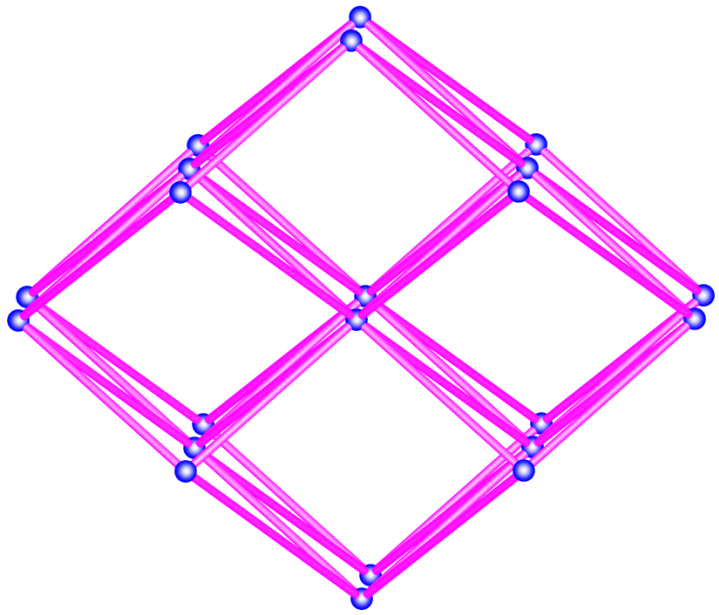


**Fig. 11** The eight-connected topological structure of type B in which the nodes represent  $\text{Ni}_3$  segments, the pink bonds represent  $1,4\text{-ndc}^{2-}$  bridges.

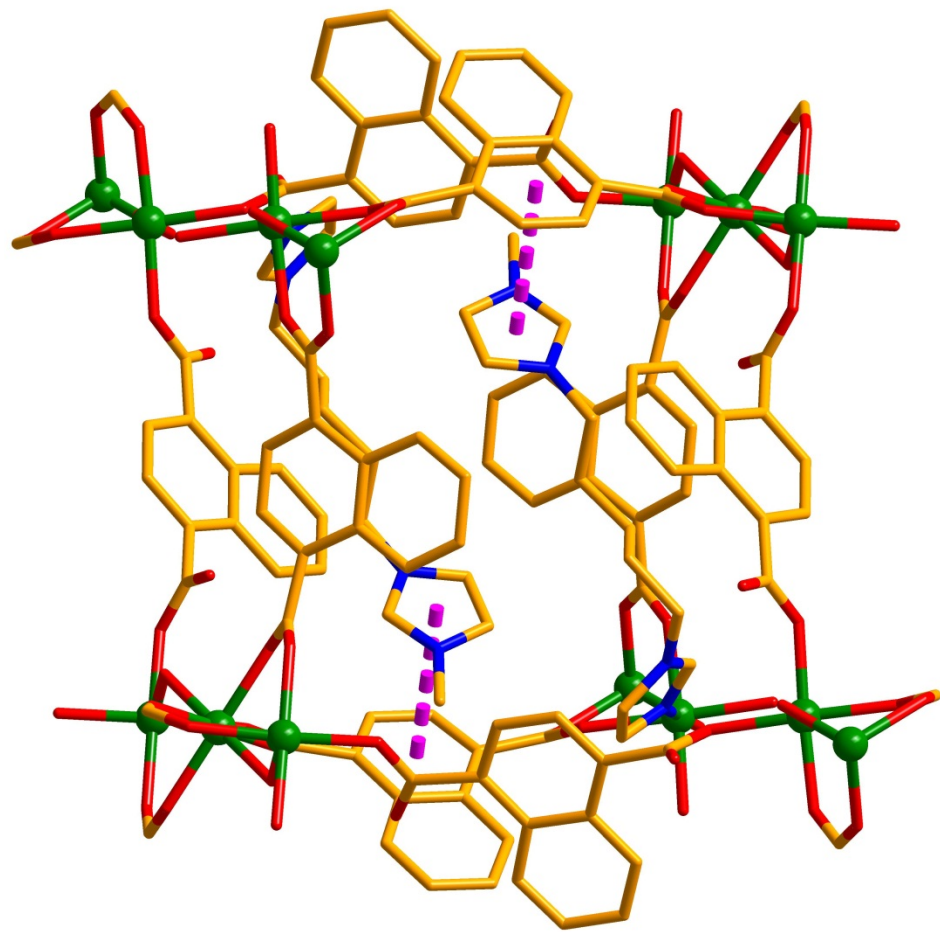


**Figure S12.** View of  $\pi\cdots\pi$  interactions between benzene rings of 1,4-ndc<sup>2-</sup> ligands and imidazole rings of [MIm-C<sub>5</sub>Im]<sup>2+</sup> cations in **3**.

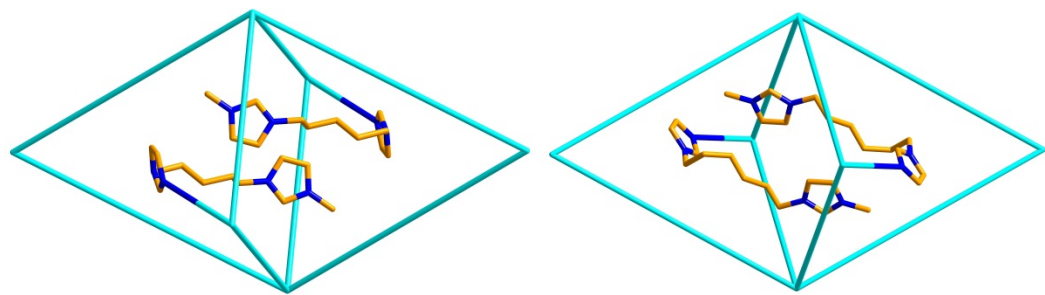


**Figure S13.**  $[\text{MIm-C}_5\text{Im}]^{2+}$  and  $[\text{MIm-C}_6\text{Im}]^{2+}$  cations act as flexible ligands coordinating to Ni(II) ions and fill the void space.

#### 4. Additional Measurements.

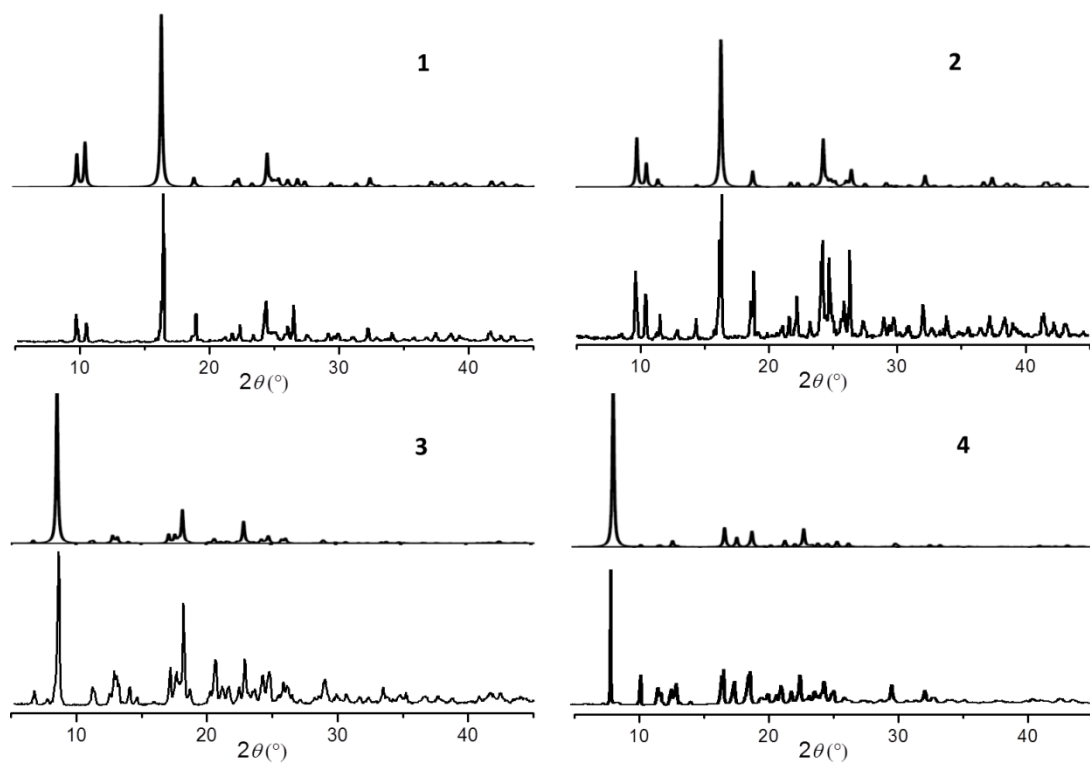


**Figure S14.** The X-ray powder diffraction (XRPD) patterns that of the bulk samples (down) and those calculated from the single-crystal diffraction data (up) for **1-4**.

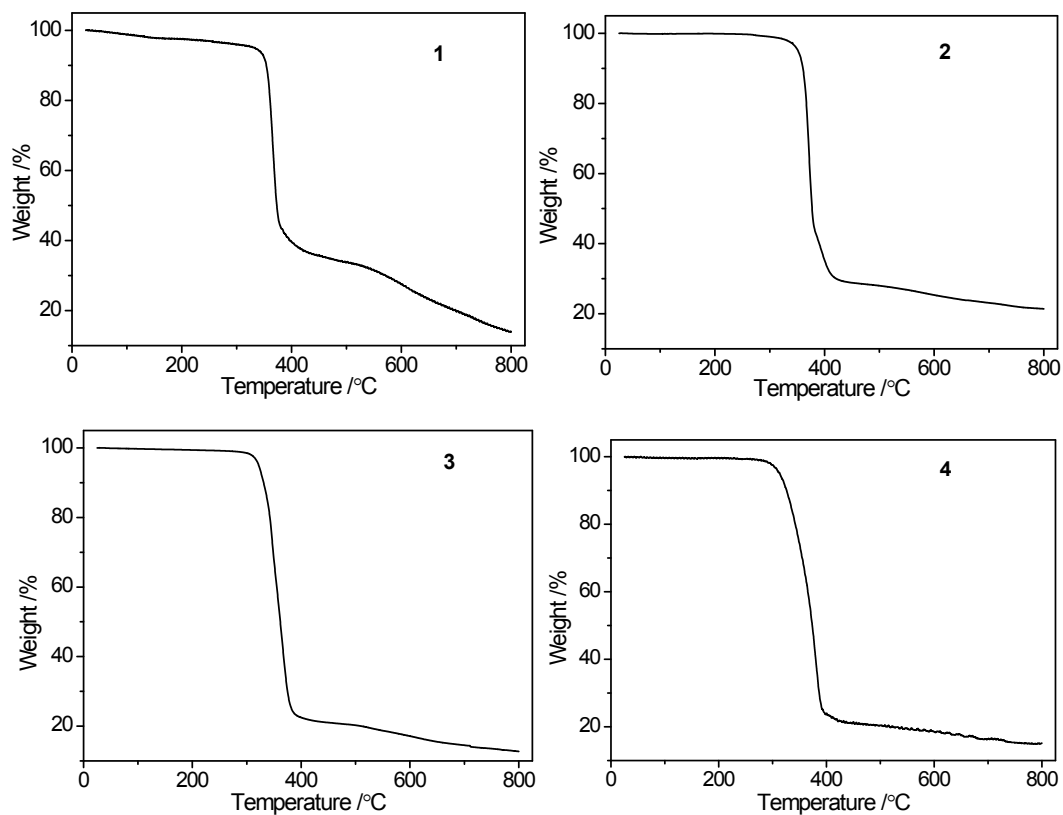


**Figure S15.** TGA curves for polymers **1–4**.

## 5. Magnetic properties.

*Polymer 1.* The distance between two nickel(II) ions within a dimer unit is 2.85 Å of **1**, which is smaller than 3 Å, suggesting that the existence of the super-exchange coupling interactions among the metal centers. The thermal variation of the product of the molar magnetic susceptibility times temperature ( $\chi_M T$ ) per Ni(II) dimer for polymer **1** shows at room temperature a value of 2.41 cm<sup>3</sup> mol<sup>-1</sup> K, close to the expected spin-only value for two isolated  $S = 1$  Ni(II) ions (2 cm<sup>3</sup> mol<sup>-1</sup> K). Upon cooling,  $\chi_M T$  value gradually approaches a value of 2.31 cm<sup>3</sup> mol<sup>-1</sup> K at 72 K and rapidly decreases to 2.04 cm<sup>3</sup> mol<sup>-1</sup> K. The fitting of Curie-Weiss law above 125 K gives  $C = 2.45$  cm<sup>3</sup> mol<sup>-1</sup> K and  $\theta = -6.42$  K. This behavior indicates that polymer **1** presents a dominant antiferromagnetic Ni–Ni exchange coupling inside its dimeric structure.

Since the structure of **1** shows the presence of well-isolated paddlewheel Ni(II) dimers connected through carboxyl groups, the magnetic data of **1** can be analyzed using the Bleaney-Bowers (eq 1) derived from the isotropic spin Heisenberg Hamiltonian  $H = -JS_1S_2$  with local spin  $S = 1$  Ni(II):

$$\chi_M = (1-c) \frac{Ng^2\beta^2}{kT} \frac{2e^{2J/kT} + 10e^{6J/kT}}{1+3e^{2J/kT} + 5e^{6J/kT}} + c \frac{2Ng^2\beta^2}{3kT} \quad 1$$

This simple model gives a very satisfactory fit of the magnetic properties of **1** in the whole temperature range with the following set of parameters:  $g = 2.94$ ,  $J = -29.76$  cm<sup>-1</sup>, paramagnetic  $S = 1$  impurity of  $c = 8.32\%$  and  $R = 1.6 \times 10^{-7}$  (R is the agreement factor defined as  $R = \Sigma[(\chi_M)^{\text{exp.}} - (\chi_M)^{\text{calcd.}}]^2 / \Sigma(\chi_M)^{\text{exp.}}^2$ ). The exchange-coupling interactions within a dimer are antiferromagnetic interaction for Ni(II).

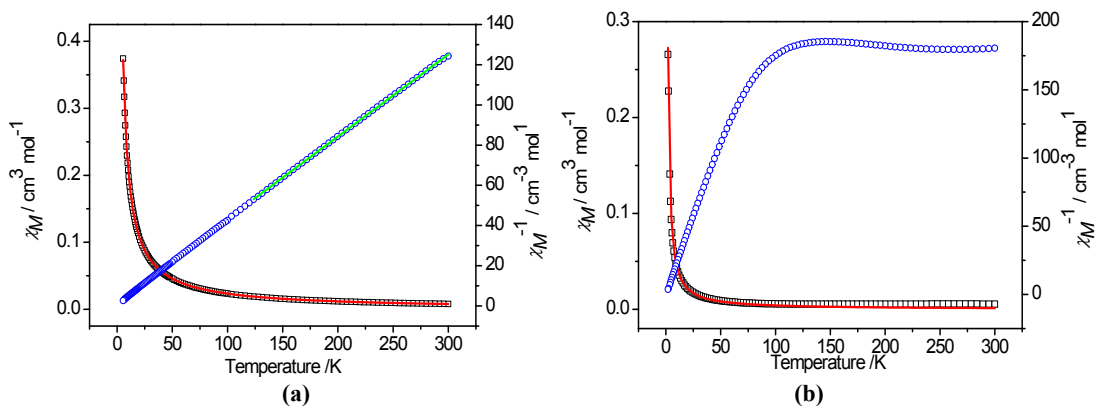


**Figure S16.** (a) Molar magnetic susceptibility of **1** as  $\chi_M$  and  $\chi_M^{-1}$  vs  $T$ . Green solid line is generated from the best fit by the Curie-Weiss expression and red solid line represents the fit to the  $\chi_M$  experimental parameters.. (b) Molar magnetic susceptibility of **2** as  $\chi_M$  vs  $T$ . The red solid line is the fit to the  $\chi_M$  experimental parameters (Polymer **2** does not fit Curie-Weiss Law).

*Polymer 2.* Similar to **1**, the distance between two metal ions within a dimer unit is 2.84 Å, suggesting that the existence of the strong super-exchange coupling interactions among the metal centers as well. As shown in Figure 2, the  $\chi_M T$  value of **2** at room temperature is 0.83 cm<sup>3</sup> mol<sup>-1</sup> K ( $\chi_M$  is the molar magnetic susceptibility per Ni(II) ion), slightly less than the spin-only value of 1 cm<sup>3</sup> mol<sup>-1</sup> K for Ni(II) non-interacting ion, indicating the presence of dominant antiferromagnetic exchange interactions. When the sample is cooled,  $\chi_M T$  shows a continuous decrease starting at room temperature to reach a value of ca. 0.431 cm<sup>3</sup> K mol<sup>-1</sup> at 18 K, and then a tiny rise at very low temperatures. The behavior described above is consistent with the occurrence of antiferromagnetic coupling between the two  $S = 1$  centers and the existence of a small paramagnetic impurity.

The magnetic data of paddlewheel Ni(II) dimers **2** can also be analyzed by Bleaney-Bowers model (eq 1) and gives a good fit in the whole temperature range with the following set of parameters:  $g = 2.14$ ,  $J = -3.44$  cm<sup>-1</sup>, paramagnetic  $S = 1$  impurity of  $c = 11.90\%$  and  $R = 8.5 \times 10^{-6}$ .

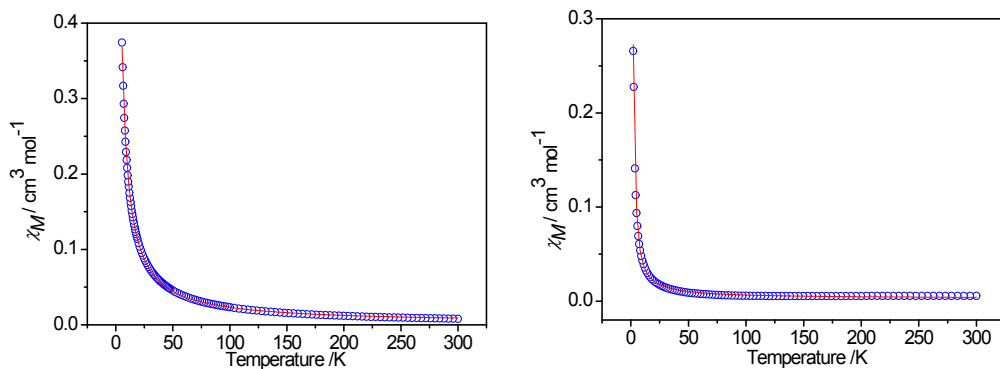


**Figure S17.** The fit of molar magnetic susceptibility in **1** (left) and **2** (right) with considering ZFS by eq 2.

Since divalent nickel can have a large zero-field splitting parameter ( $D$ ), the occurrence of ZFS in the  $S = 1$  local spin state was explicitly taken into account as reported by Ginsberg *et al.*<sup>1</sup> Let the system be quantized along the  $z$  direction and assume axial symmetry. In the absence of a magnetic field and neglecting interdimer interaction, the Hamiltonian is  $\mathbf{H} = -J\mathbf{S}_1\mathbf{S}_2 - D(\mathbf{S}_{1z}^2 + \mathbf{S}_{2z}^2)$ . We obtain for the field-independent susceptibilities:

$$\chi_M = \frac{Ng^2\beta^2}{3k} \left\{ \frac{F1}{T} + \frac{2}{D}F2 + \frac{6C2^2}{3J-\delta}F3 + \frac{6Cl^2}{3J+\delta}F4 \right\} + N\alpha \quad 2$$

where

$$\begin{aligned}\delta &= \left[ (3J+D)^2 - 8JD \right]^{1/2} \\ C1 &= 2\sqrt{2}D / \left[ (9J-D+3\delta)^2 + 8D \right]^{1/2} \\ C2 &= (9J-D+3\delta) / \left[ (9J-D+3\delta)^2 + 8D \right]^{1/2}\end{aligned}$$

$$F1 = \frac{1 + e^{4J/kT} + 4e^{(4J+D)/kT}}{2 + e^{D/kT} + e^{(J-\delta)/kT} + e^{(J+\delta)/kT} + 2e^{4J/kT} + 2e^{(4J+D)/kT}}$$

$$F2 = \frac{2e^{(4J+D)/kT} + e^{D/kT} - 1 - 2e^{4J/kT}}{2 + e^{D/kT} + e^{(J-\delta)/kT} + e^{(J+\delta)/kT} + 2e^{4J/kT} + 2e^{(4J+D)/kT}}$$

$$F3 = \frac{e^{4J/kT} - e^{(J+\delta)/kT}}{2 + e^{D/kT} + e^{(J-\delta)/kT} + e^{(J+\delta)/kT} + 2e^{4J/kT} + 2e^{(4J+D)/kT}}$$

$$F4 = \frac{e^{4J/kT} - e^{(J-\delta)/kT}}{2 + e^{D/kT} + e^{(J-\delta)/kT} + e^{(J+\delta)/kT} + 2e^{4J/kT} + 2e^{(4J+D)/kT}}$$

$N\alpha$  is a correction term for the temperature-independent paramagnetism.

The magnetic data were analyzed by eq 2 with considering ZFS and gives a good fit in the whole temperature range with the following set of parameters: for **1**,  $g = 2.85$ ,  $J = -21.57$  cm<sup>-1</sup>,  $D = 1.06$  cm<sup>-1</sup>,  $N\alpha = 1.9 \times 10^{-3}$  and  $R = 1.3 \times 10^{-6}$ ; for **2**,  $g = 2.21$ ,  $J = -19.92$  cm<sup>-1</sup>,  $D = 23.51$  cm<sup>-1</sup>,  $N\alpha = 2.8 \times 10^{-3}$  and  $R = 3.2 \times 10^{-6}$ . Because polymer **2** has a large  $D$  value, the magnetic coupling may include a big zero field splitting (ZFS) contribution.

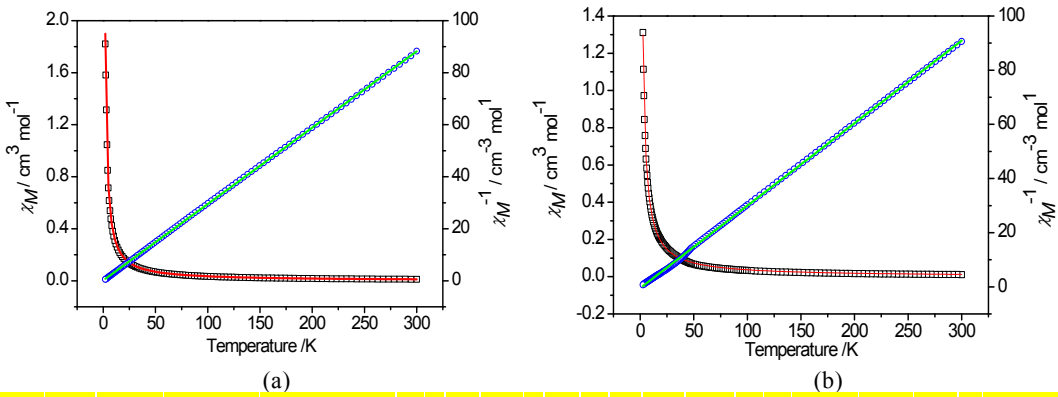


**Figure S18.** Molar magnetic susceptibility of **1** (a) and **2** (b) as  $\chi_M$  and  $\chi_M^{-1}$  vs  $T$ . Green solid line is generated from the best fit by the Curie–Weiss expression and the red solid line represents the fit data by eq 3.

**Polymer 3.** Fig.S18 shows the temperature dependence of the  $\chi_M$  and  $\chi_M^{-1}$  values for **3**. As can be seen, **3** shows a room-temperature  $\chi_M T$  value of 3.40 cm<sup>3</sup> mol<sup>-1</sup> K per Ni(II) trimer. When the temperature is lowered, the  $\chi_M T$  decreases to minimum value of 3.35 cm<sup>3</sup> mol<sup>-1</sup> K at 63 K, then rises sharply to a maximum value of 3.95 cm<sup>3</sup> mol<sup>-1</sup> K at 4 K. The fitting of Curie-Weiss law in the whole temperature range gives  $C = 3.41$  cm<sup>3</sup> mol<sup>-1</sup> K and  $\theta = 0.52$  K, indicating that intermetallic magnetic interaction is weakly ferromagnetic. Since the structure of **3** shows the presence of well-isolated centrosymmetric linear Ni(II) trimers, we have fitted the magnetic properties of to the simple model derived for a centrosymmetrical  $S=1$  linear trimer with the Hamiltonian  $H = -2J(S_1S_2 + S_2S_3) - J'S_1S_3$ , where  $S_2$  is the spin state of the central Ni(II) ion, the exchange coupling constant between the terminal ions is considered as negligible ( $J' = 0$ ) and  $J$  represents the exchange coupling constant between neighboring nickel centers :

$$\chi_M = \frac{Ng^2\beta^2}{kT} \frac{28e^{4J/kT} + 10e^{-2J/kT} + 2e^{-6J/kT} + 10e^{2J/kT} + 2}{7e^{4J/kT} + 8e^{-2J/kT} + 3e^{-6J/kT} + 5e^{2J/kT} + e^{-4J/kT} + 3} \quad 2$$

This above model gives a good fit in the whole temperature range with the following set of parameters:  $g = 2.18$ ,  $J = 2.78 \text{ cm}^{-1}$  and  $R = 2.2 \times 10^{-4}$ . The obtained  $J$  value is positive, consistent with the presence of weak Ni(II)–Ni(II) ferromagnetic interaction.

The structure of **3** shows that three Ni(II) are connected by an aqua and a carboxylate bridge. For the aqua pathways, the Ni–O–Ni bond angles are  $113.6^\circ$ , out of the range  $80$ – $100^\circ$  for ferromagnetic coupling. Hence, the overall ferromagnetic interacion should be originated from the ferromagnetic contribution of carboxylate bridges that is larger than the antiferromagnetic contribution of aqua bridges.<sup>2</sup>

*Polymer 4.* The room-temperature  $\chi_M T$  value of  $3.31 \text{ cm}^3 \text{ mol}^{-1} \text{ K}$  per Ni(II) trimer. When the temperature is lowered, the  $\chi_M T$  curve goes stable, and upon cooling rapidly increases to a maximum  $3.83 \text{ cm}^3 \text{ mol}^{-1} \text{ K}$  at  $24 \text{ K}$  and then abrupt decreases. The fitting of Curie-Weiss law gives  $C = 3.28 \text{ cm}^3 \text{ mol}^{-1} \text{ K}$  and  $\theta = 1.56 \text{ K}$ , indicating that the magnetic interaction is weakly ferromagnetic. As described above, the eq2 is appropriate to **4** which is isostructural to **3** with well-isolated centrosymmetric linear Ni(II) trimers. This above model gives a good fit in the whole temperature range with the following set of parameters:  $g = 2.27$ ,  $J = 4.88 \text{ cm}^{-1}$  and  $R = 2.0 \times 10^{-5}$ , suggesting weak ferromagnetic couplings.

As also observed in polymer **3** and **4**, attempts to fit both parameters (ZFS and antiferromagnetic coupling) result in unrealistic values since both factors are highly correlated and the magnetic coupling is weak.

## References:

1. A. P. Ginsberg, R. L. Martin, R. W. Brookes and R. C. Sherwood, *Inorg. Chem.*, 1972, **11**, 2884-2889.
2. J. Yang, G.-B. Che, B. Liu, Y.-Y. Liu and J.-F. Ma, *Inorg. Chem. Commun.*, 2010, **13**, 112-115.